An Impedance-based Parameter Design Method for Active Damping of Load Converter Station in MTDC Distribution System

Pengwei Chen, *Member*, *IEEE*, Wenmeng Zhao, Xin Chen, *Member*, *IEEE*, and Wenwei Jiang

***Abstract*—To achieve the efficient application of impedance analysis in the stability assessment and enhancement of multi-terminal DC distribution systems, this paper proposes the DC-side reduced-order impedance models with power control and AC voltage control, respectively, by taking the load converter station as the object. By using the DC-side current as the feed-forward state, the active compensator applied to the load converter station with two control modes is also derived as well as the corresponding reduced-order impedance models. Combined with the reduced-order impedance models, a method based on damping factor sensitivity is further proposed to design the parameters of the derived active compensators. The verification results in the frequency domain and time domain demonstrate the accuracy of the reduced-order impedance and the effectiveness of the proposed compensator parameter design method.**

***Index Terms*—Impedance modeling, order reduction, active compensator, damping factor, sensitivity.**

I. Introduction

With the rapid development of semiconductor devices and control technologies in previous decades, the DC distribution network based on the voltage source converter (VSC) [1], especially multi-terminal DC (MTDC) systems, has become an attractive alternative to enable the efficient integration of distributed generators (DGs) and DC loads [2], [3]. According to the difference in the energy flow into or out of the DC network, VSC stations in the MTDC system can be classified into two types: source converter station and load converter station. The load converter station connected to an active network can operate in the power control mode, while the station supplying power to a passive network generally adopts the AC voltage control. Whether under power control or AC voltage control, the load converter station possesses the property of a constant-power load [4]-[6], which would result in stations encountering interaction problems, such as low-frequency oscillations [7]. Therefore, the stability, especially small-signal stability, is a fundamental issue in the operation of MTDC distribution systems, and stability enhancement, such as the active damping control, is required in many cases [8], [9].

In addition to the time-domain simulation, there are two main categories of methods to assess the small-signal stability, namely state-space analysis and impedance analysis [10]-[12]. Although the former method provides insight into multi-converter interactions through the participation factor and sensitivity analysis, it still relies on the complicated full-state small-signal model, where the model order will increase dramatically as the number of converters increases [13]. Once the MTDC distribution network operates in different modes or structures, the state-space model needs to be rebuilt, thus leading to a huge amount of work. The impedance analysis, which is a well-established technique employed to analyze interconnected systems [14], has gained increasing popularity in recent years. The ratio of the source output impedance to the load input impedance is primarily used to satisfy the Nyquist stability criterion or other improved criteria [15], [16]. Thus, the impedance modeling of the terminal has become a key point in the application of impedance analysis.

To achieve the accurate modeling for DC-side impedance, various models and methods have been proposed from different perspectives [17]-[20]. Based on the power balance between the AC and DC sides, the DC-side impedance models of the rectifier and inverter stations are derived in [17] to analyze the stability of a two-terminal DC system, but the modeling only involves the power and DC voltage control. In [18], the VSC-based high-voltage direct current (VSC-HVDC) system is represented as a feedback interconnection of two subsystems that are defined as a VSC DC-side power dependent admittance and DC-network impedance, respectively. Such a modeling approach helps provide the physical meaning of instability; however, the modeling process still depends on the full-order state-space equations. To enhance the universality for VSCs with different control tasks, a com-

Manuscript received: February 1, 2021; revised: April 19, 2021; accepted: June 10, 2021. Date of CrossCheck: June 10, 2021. Date of online publication: September 24, 2021.

This work was supported in part by the National Natural Science Foundation of China (No. 52007080), the China Postdoctoral Science Foundation (No. 2020TQ0142), and the Opening Foundation of State Key Laboratory of Alternate Electrical Power System with Renewable Energy Sources (No. LAPS21008).

P. Chen (corresponding author), W. Zhao, X. Chen, and W. Jiang are with the Jiangsu Key Laboratory of New Energy Generation and Power Conversion, College of Automation Engineering, Nanjing University of Aeronautics and Astronautics, Nanjing, China (e-mail: chenpw2019@nuaa.edu.cn; wmzhao0524@163.com; chen.xin@nuaa.edu.cn; jiangww0121@163.com).

DOI: 10.35833/MPCE.2021.000096

prehensive DC-side impedance model for conventional three-phase two-level VSC in different control modes is proposed in [19], and the effects of controller parameters are also analyzed in detail. In [20], the DC-side small-signal impedance model of the modular multilevel converter is established by using the harmonic linearization, which has a higher accuracy than that in the *dq* reference frame.

For emphasis, whether based on conventional state space or harmonic state space, the above impedance models and their derivation processes are all complicated. For ease of application, various reduced-order impedance models have been explored for different DC systems and control modes [21]-[24]. The common idea to establish the reduced-order model is to approximate or ignore the fast-current control dynamics, the effect of the AC-side voltage and *q*-axis current, and even the outer loop regulator. An extreme case is that the converter with AC voltage control is represented by a negative resistance. In the research scenario of low-frequency oscillation, the above reduced-order methods can generate an impedance model with satisfactory performance, but its accuracy will decay as the frequency of the oscillation problems increases. Besides, the impedance model integrates all the dynamics of the converter and thus promotes the efficient stability assessment, but some critical information on oscillation characteristics, which can indicate the trends related to the changes of parameters and operating conditions, are also hidden in the modeling and analysis process. In essence, this hinders their application. Although the impedance reshaping by the optimization of the controller parameter has been applied to the grid-connected inverter and DC system in [24]-[26], it is difficult to accurately determine the impedance intersection frequency and phase margin, which are required in phase compensation, and it is also difficult to obtain a clear adjustment direction of compensator parameters. Besides, such a remodeling method requires that the input impedance of the inverter has no right half plane (RHP) zeros, which leads to some application limitations.

From the perspective of stability assessment and enhancement using the impedance analysis, especially in the parameter design of active damping, it is often desirable that the complex full-order impedance model can be approximated by a reduced-order formulation, and the method for parameter adjustment to improve stability can be revealed.

Motivated by the above requirements, this paper proposes a method based on reduced-order impedance and damping factor sensitivity to design the parameter in the active damping strategy of the load converter station. The main contributions are drawn as follows.

1) Based on the detailed DC-side small-signal impedance modeling of the load converter station, the order reduction conditions of model are analyzed, and the reduced-order impedance models under the power and AC voltage control as well as the impedance characteristics are then investigated.

2) Taking the DC-side current as the feedforward state, the active compensators applied to the load converter station are deduced from the parallel virtual resistance, and the DC-side reduced-order impedance models are given with additional active damping corresponding to two control modes.

3) By using the reduced-order impedance models and the damping factor sensitivity, a method to design the parameters of the deduced active compensators is further proposed.

The remainder of this paper is organized as follows. Section II introduces the full-order small-signal impedance model formulated by state-space equations, the order reduction conditions of impedance model, and the DC-side reduced-order impedance models in two control modes. Section III presents the derivation process of active compensators applied to the load converter station, the corresponding impedance models, and the parameter design method based on the damping factor sensitivity. The case studies are discussed in Section IV, and Section V concludes this paper.

II. Impedance Model of Load Converter Station

The typical formulation of load converter station connected to an active network and passive network is shown in Fig. 1(a), where the active network is represented by a Thevenin equivalent circuit with an equivalent internal impedance of R_g and L_g, whereas the passive network is equivalent to the impedance Z_{load}. In the common part of the two application scenarios, C_s is the DC-link capacitor; R_f is the equivalent resistance at the bridge side; and L_f and C_f are the filter inductor and capacitor, respectively.

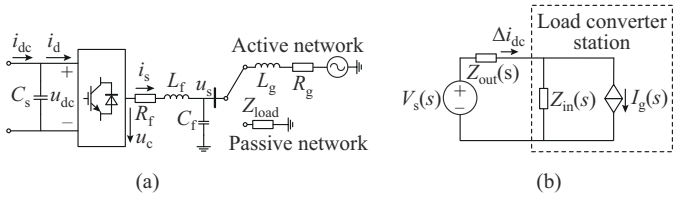

Fig. 1. Basic structure of load converter station and its equivalent circuit. (a) Basic structure of load converter station. (b) Small-signal equivalent circuit.

A. Full-order Small-signal Impedance

In three-phase stationary coordinates, the AC- and DC-side dynamics of the converter station can be described as:

$$\begin{cases} sL_f \boldsymbol{I}_{sabc} = -R_f \boldsymbol{I}_{sabc} + \boldsymbol{U}_{cabc} - \boldsymbol{U}_{sabc} \\ sC_s u_{dc} = i_{dc} - \boldsymbol{I}_{sabc}^{T} \boldsymbol{U}_{cabc} / u_{dc} \end{cases} \tag{1}$$

where $\boldsymbol{I}_{sabc}$, $\boldsymbol{U}_{cabc}$, and $\boldsymbol{U}_{sabc}$ are the vectors of three-phase current, the output voltage of converter, and the grid-side voltage, respectively; and u_{dc}, i_{dc}, and s are the DC-side voltage, DC-side current, and Laplacian operator, respectively.

By introducing the park transformation matrix (*d*-axis lags *q*-axis) in (1) and linearizing it at a given equilibrium point, the small-signal equations of the main circuit for the load converter station in *dq* coordinates can be obtained as:

$$\begin{cases} sL_f \Delta i_{sd} = -R_f \Delta i_{sd} + \omega_0 L_f \Delta i_{sq} + \Delta u_{cd} - \Delta u_{sd} \\ sL_f \Delta i_{sq} = -R_f \Delta i_{sq} - \omega_0 L_f \Delta i_{sd} + \Delta u_{cq} - \Delta u_{sq} \\ sC_s \Delta u_{dc} = \Delta i_{dc} - \Delta P / u_{dc0} + i_{dc0} \Delta u_{dc} / u_{dc0} \end{cases} \tag{2}$$

where i_s, u_c, and u_s are the filter inductor current, output voltage of converters, and grid-side voltage, respectively; symbol Δ denotes a small-signal change in a variable; subscripts

d and q denote the d- and q-axis values, respectively; subscript 0 denotes the steady-state value of state variables; ω_0 is the angular frequency of the utility grid; and $\Delta P = 1.5(i_{sd0}\Delta u_{cd} + u_{cd0}\Delta i_{sd} + i_{sq0}\Delta u_{cq} + u_{cq0}\Delta i_{sq})$.

According to the power stage model in (2), we have:

$$\Delta u_{dc} = G_1(s)\Delta i_{sd} + G_2(s)\Delta i_{dc} + G_3(s)\Delta u_{cd} + G_4(s)\Delta i_{sq} + G_5(s)\Delta u_{cq} \tag{3}$$

$$\begin{cases} G_1(s) = \dfrac{\Delta u_{dc}}{\Delta i_{sd}} = -\dfrac{1.5u_{cd0}}{su_{dc0}C_s - i_{dc0}} \\ G_2(s) = \dfrac{\Delta u_{dc}}{\Delta i_{dc}} = \dfrac{u_{dc0}}{su_{dc0}C_s - i_{dc0}} \\ G_3(s) = \dfrac{\Delta u_{dc}}{\Delta u_{cd}} = -\dfrac{1.5i_{sd0}}{su_{dc0}C_s - i_{dc0}} \\ G_4(s) = \dfrac{\Delta u_{dc}}{\Delta i_{sq}} = -\dfrac{1.5u_{cq0}}{su_{dc0}C_s - i_{dc0}} \\ G_5(s) = \dfrac{\Delta u_{dc}}{\Delta u_{cq}} = -\dfrac{1.5i_{sq0}}{su_{dc0}C_s - i_{dc0}} \end{cases} \tag{4}$$

Combined with the classic configuration of the power control scheme, the small-signal model of the load converter station is shown in Fig. 2, where $G_{LP}(s)$ is the low-pass filter of a measurement that can be added on demand; P and Q are the active and reactive power, respectively; superscript * denotes the reference value; $G_p(s)$ and $G_i(s)$ are the outer- and inner-loop regulators, respectively; and k_{pwm} and T are the modulation gain and switching cycle, respectively.

By using state-space representation, the small-signal model of the load converter station with power control can be formed as:

$$\begin{cases} s\Delta \boldsymbol{x}_{pc} = \boldsymbol{A}_{pc}\Delta \boldsymbol{x}_{pc} + \boldsymbol{B}_{pc}\Delta \boldsymbol{u}_{pc} \\ \Delta \boldsymbol{y}_{pc} = \boldsymbol{C}_{pc}\Delta \boldsymbol{x}_{pc} + \boldsymbol{D}_{pc}\Delta \boldsymbol{u}_{pc} \end{cases} \tag{5}$$

where $\Delta \boldsymbol{x}_{pc}$, $\Delta \boldsymbol{u}_{pc}$, and $\Delta \boldsymbol{y}_{pc}$ are the state vector, input vector, and output vector, respectively; and $\boldsymbol{A}_{pc}$, $\boldsymbol{B}_{pc}$, $\boldsymbol{C}_{pc}$, and $\boldsymbol{D}_{pc}$ are the state matrix, control matrix, output matrix, and direct transfer matrix, respectively. The expressions of these matrices can be easily derived by (2)-(4) and the control loop, which are not listed in this paper owing to space limitations.

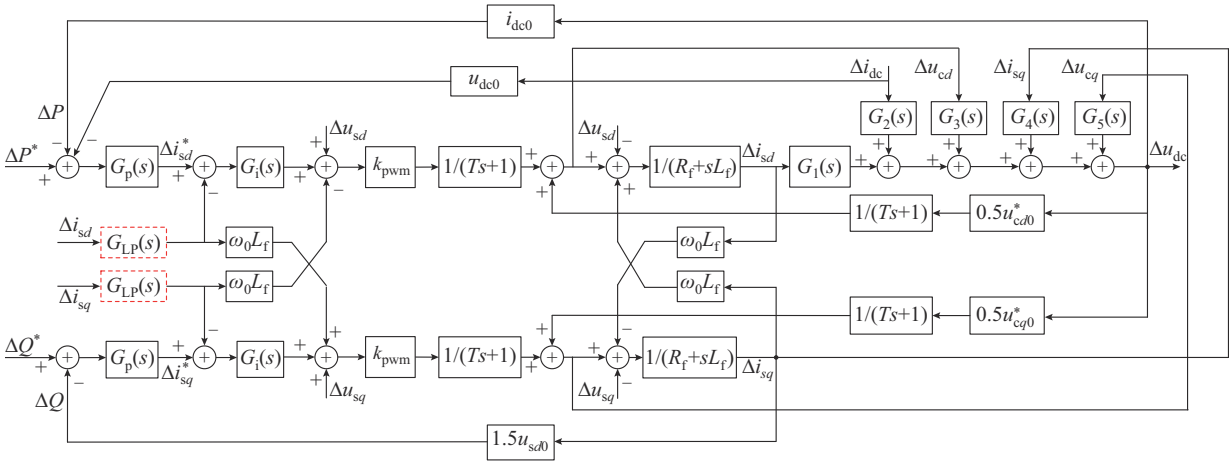

Fig. 2. Small-signal model of load converter station with power control.

Let Δu_{dc} represents the observed quantity, then the transfer function form of equation (5) can be derived as:

$$\boldsymbol{H}(s) = \frac{\Delta u_{dc}}{\Delta \boldsymbol{u}_{pc}} = \boldsymbol{C}_{pc}(s\boldsymbol{I} - \boldsymbol{A}_{pc})^{-1}\boldsymbol{B}_{pc} + \boldsymbol{D}_{pc} \tag{6}$$

where $\boldsymbol{I}$ is the unit matrix. Let Δi_{dc} represent the input quantity, the DC-side full-order small-signal impedance can be derived as $Z_{pc0}(s) = \Delta u_{dc}/\Delta i_{dc}$.

Remark 1: comparing the capacities of the MTDC distribution system and AC transmission system, the load converter station connected to the active network can be considered to be connected to a strong AC source. Its equivalent internal impedance is small, and the system frequency is highly stable. With this assumption, u_{sdq} can be regarded as a constant, i.e., $\Delta u_{sdq} = 0$, and the phase-locked loop (PLL) has little effect on the small-signal stability of the DC system [27]. To obtain the small-signal model and impedance model as concisely as possible, the performance of the PLL is considered extremely ideal, and its modeling process is neglected. The full-order impedance model of the load converter station with AC voltage control, namely $Z_{vc0}(s)$, can be obtained using a similar process. However, the derivation involves many state variables and the inverse operation of the matrix, which means that the analytical expression with symbolic variables is still complicated and difficult to deal with.

B. Reduced-order Impedance with Power Control

It is well-known that MTDC, which is a typical power electronic-based system, has a two time-scale property in nature. To achieve the efficient analysis of the low-frequency phenomenon, this section investigates the low-complexity DC-side small-signal impedance model of the load converter station. As shown in Fig. 2, the order reduction conditions can be summarized as follows.

1) The digital control delay $1/(Ts+1)$ usually has a large bandwidth, and we can assume that it only affects the impedance in the high-frequency band, while in the low-frequency band, it can be equivalent to the unity gain.

2) The dq-axis current controller prompts Δi_{sd} and Δi_{sq} are

independently controlled by Δi_{sd}^{*} and Δi_{sq}^{*}, and the term $\omega_0 L_f$ in decoupling feedforward and AC-side dynamics can be removed. This approach is usually adopted in literature for the convenience of analysis [28].

3) The dynamic of the capacitor voltage relies on the power balance between the AC and DC sides, which essentially comprises a multi-input multi-output segment. A common use is to neglect the Δu_{cdq} and Δi_{sq}, and only Δi_{sd} is preserved to determine ΔP [21].

After these simplifications, we can obtain:

$$\begin{cases} (\Delta P^{*} - i_{dc0}\Delta u_{dc} - u_{dc0}\Delta i_{dc})G_p(s) = \Delta i_{sd}^{*} \\ (\Delta i_{sd}^{*} - \Delta i_{sd})G_i(s)k_{pwm} + 0.5u_{cd0}^{*}\Delta u_{dc} = Z_f \Delta i_{sd} \\ \Delta i_{sd}G_1(s) + \Delta i_{dc}G_2(s) = \Delta u_{dc} \end{cases} \tag{7}$$

where $Z_f = R_f + sL_f$.

Removing the intermediate variables Δi_{sd} and Δi_{sd}^{*}, the DC-side impedance $Z_{pc1}=\Delta u_{dc}/\Delta i_{dc}$ can be expressed as:

$$Z_{pc1}(s) = \frac{G_2(s)(Z_f + G_i(s)k_{pwm}) - G_1(s)u_{dc0}G_p(s)G_i(s)k_{pwm}}{Z_f + G_i(s)k_{pwm} + G_1(s)(i_{dc0}G_p(s)G_i(s)k_{pwm} - 0.5u_{cd0}^{*})} \tag{8}$$

Obviously, the order reduction above is a truncation approach, which is too rough to guarantee the accuracy of the impedance model as the q-axis control still has a certain impact on the d-axis control. A preferred approach is to approximate the dynamics of Δu_{cdq} and Δi_{sdq} as much as possible.

When the load converter station adopts the unity power factor control, namely $i_{sq0}=0$, we have:

$$\begin{cases} i_{sd0} \neq 0, u_{cq0} \neq 0, i_{sq0} = 0 \\ G_3(s) \neq 0, G_4(s) \neq 0, G_5(s) = 0 \end{cases} \tag{9}$$

Even without configuring the unity power factor control, the influence of Δu_{cq} can still be ignored as long as the reactive current is small enough, and then (2) can be rewritten as:

$$\begin{cases} \Delta u_{cd} = (Z_f + \omega_0^2 L_f^2 / Z_f)\Delta i_{sd} = U_{cd,pc}(s)\Delta i_{sd} \\ \Delta i_{sq} = -\omega_0 L_f / Z_f \Delta i_{sd} = I_{sq,pc}(s)\Delta i_{sd} \end{cases} \tag{10}$$

After Δu_{cd} and Δi_{sq} are represented by Δi_{sd}, the small-signal model of the load converter station with power control shown in Fig. 2 can be simplified, as shown in Fig. 3(a). By performing order reduction in this way, the DC-side impedance $Z_{pc2}(s)$ can be expressed as:

$$Z_{pc2}(s) = \frac{-u_{dc0}G_p(s)H_1(s) + G_2(s)}{1 - H_1(s)H_2(s)} \tag{11}$$

$$\begin{cases} H_1(s) = \dfrac{G_i(s)k_{pwm}(G_1(s) + U_{cd,pc}(s)G_3(s) + I_{sq,pc}(s)G_4(s))}{G_i(s)k_{pwm} + Z_f} \\ H_2(s) = \dfrac{0.5u_{cd0}^{*}}{G_i(s)k_{pwm}} - i_{dc0}G_p(s) \end{cases} \tag{12}$$

Remark 2: if the control scheme is configured with the low-pass signal filters, as shown in Fig. 2, the corresponding reduced-order impedance model can be obtained by inserting the block marked with red dotted lines into the feedback loop of Fig. 3(a).

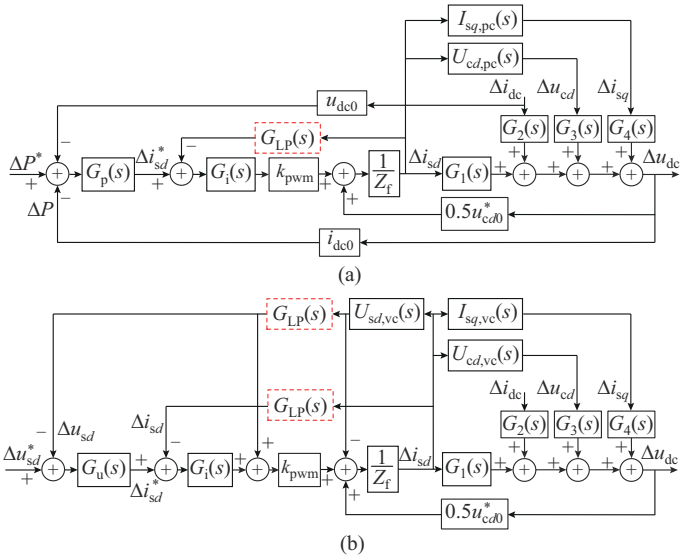

Fig. 3. d-axis control block diagram of load converter station. (a) With power control. (b) With AC voltage control.

C. Reduced-order Impedance with AC Voltage Control

The load converter station connected to the passive network needs to establish the AC-side voltage by itself. The AC voltage is significantly affected by the load current, which means the approximation applied to AC voltage control is different from that applied to power control. Under the assumption that the passive network is equivalent to Z_{load}, the dynamic state of the passive network can be expressed as:

$$\begin{cases} \Delta i_{sd} = sC_f\Delta u_{sd} - \omega_0 C_f \Delta u_{sq} + \Delta u_{sd}/Z_{load} \\ \Delta i_{sq} = sC_f\Delta u_{sq} + \omega_0 C_f \Delta u_{sd} + \Delta u_{sq}/Z_{load} \end{cases} \tag{13}$$

Considering that the capacity of the filter capacitor C_f is small, the coupling effect caused by the filter is ignored, and the d-axis voltage can be simplified as:

$$\Delta u_{sd} = \Delta i_{sd}\frac{Z_{load}}{sC_f Z_{load} + 1} = U_{sd,vc}(s)\Delta i_{sd} \tag{14}$$

Similar to the load converter station with power control, Δu_{cd} and Δi_{sq} can be represented by Δi_{sd} using (15):

$$\begin{cases} \Delta u_{cd} = \Delta u_{sd} + Z_f\Delta i_{sd} - \omega_0 L_f \Delta i_{sq} = U_{cd,vc}(s)\Delta i_{sd} \\ \Delta i_{sq} = -\omega_0 L_f / Z_f \Delta i_{sd} = I_{sq,vc}(s)\Delta i_{sd} \end{cases} \tag{15}$$

Combined with the scheme of AC voltage control, the small-signal model of the load converter station can be simplified as shown in Fig. 3(b), and then its equivalent DC-side impedance is given by:

$$Z_{vc1}(s) = \frac{\Delta u_{dc}}{\Delta i_{dc}} = \frac{G_2(s)}{1 - F_1(s)F_2(s)F_3(s)} \tag{16}$$

$$\begin{cases} F_1(s) = \dfrac{k_{pwm}G_u(s)G_i(s)}{G_i(s)k_{pwm}(1 + U_{sd,vc}(s)G_u(s)) + Z_f + (1 - k_{pwm})U_{sd,vc}(s)} \\ F_2(s) = G_1(s) + G_3(s)U_{cd,vc}(s) + G_4(s)I_{sq,vc}(s) \\ F_3(s) = \dfrac{0.5u_{cd0}^{*}}{k_{pwm}G_u(s)G_i(s)} \end{cases} \tag{17}$$

It should be noted that the impedance composition of the load converter station with AC voltage control is different

from that with power control. Its characteristics are summarized as follows.

1) $G_1(s)$, $G_3(s)$, and $G_4(s)$ all possess the low-pass characteristics such that $F_2(s)$ demonstrates the similar amplitude-frequency characteristic and its cut-off frequency is $i_{dc0}/(u_{dc0}C_s)$. According to the rated voltage and power of the MTDC system employed in Section IV, the cut-off frequency is less than 10 Hz, and the amplitude gain within the cut-off frequency can be approximated as: $1.5u_{cd0}/i_{dc0}+1.5Z_{load}i_{sd0}/i_{dc0}$.

2) Neglecting the effect of filter capacitor and inductor, $U_{sd,vc}(s)$ and $U_{cd,vc}(s)$ can be approximated by Z_{load} and $Z_{load}+Z_f$, respectively, where Z_f is very small compared with Z_{load}, and it can be further ignored. Therefore, the denominator of $F_1(s)$ is approximately equal to $Z_{load}(1-k_{pwm}+G_u(s)G_i(s)k_{pwm})$, where the amplitude is much greater than that of $F_2(s)$.

3) The denominator of $F_1(s)F_3(s)$ is the same as that of $F_1(s)$, and its numerator is $0.5u^*_{cd0}$ (roughly equivalent to 0.2 at rated voltage). When the frequency is below the cut-off frequency of $F_2(s)$, the amplitude of $F_1(s)F_2(s)F_3(s)$ is much less than 0.2, and when the frequency is higher than the cut-off frequency, the amplitude of $F_1(s)F_2(s)F_3(s)$ is close to zero.

Based on the above analysis, the denominator in (16) is simplified as constant 1, and the DC-side impedance of the load converter station with AC voltage control is approximated by:

$$Z_{vc2}(s)=G_2(s)=\frac{u_{dc0}}{su_{dc0}C_s-i_{dc0}}=-\frac{u_{dc0}}{i_{dc0}}\,/\!/\,\frac{1}{sC_s} \tag{18}$$

We can observe that (18) is essentially an impedance expression of the negative resistance $-u_{dc0}/i_{dc0}$ in parallel with a capacitor. Compared with the negative resistance derived directly from the Taylor expansion of $i=P_{const}/u_{dc}$, the simplification above indicates the origin of the negative resistance from the perspective of detailed impedance modeling.

Remark 3: through the impedance modeling of the load converter station, the small-signal equivalent circuit of the MTDC distribution system can be obtained as shown in Fig. 1(b), where the subsystem of the load converter station is represented by the input impedance $Z_{in}(s)$ (namely $Z_{pc}(s)$ or $Z_{vc}(s)$) and parallel current source $I_g(s)$, whereas the background subsystem is equivalent to a Thevenin circuit consisting of a voltage source $V_s(s)$ in series with an output impedance $Z_{out}(s)$.

III. Reduced-order Impedance Model with Active Damping and Sensitivity-based Parameter Design Method

Active damping is generally realized by adding a compensator in the control loop with state variables feedforward or feedback, thus adjusting the impedance of the load converter station. In the cascade system shown in Fig. 1(b), if the equivalent loop gain meets the Nyquist stability criterion, the small-signal stability is guaranteed. Considering this, the load converter station also has the potential to participate in the damping configuration. Therefore, the application of the active compensator to the load converter station using DC-side current feedforward is introduced in this section, and a parameter design method based on the damping factor sensitivity is also derived.

A. Reduced-order Impedance with Active Damping

To facilitate the design of an active compensator, the small-signal diagrams of the power and AC voltage control are simplified as shown in Fig. 4, where the modulation process, sampling delay, and signal filter are removed from the original, and we have

$$P_0(s)=1.5u_{cd0}+\left(\frac{Z_{load}}{sC_fZ_{load}+1}+\frac{\omega_0^2L_f^2}{Z_f}+Z_f\right)1.5i_{sd0}\approx 1.5u_{cd0}+Z_{load}1.5i_{sd0} \tag{19}$$

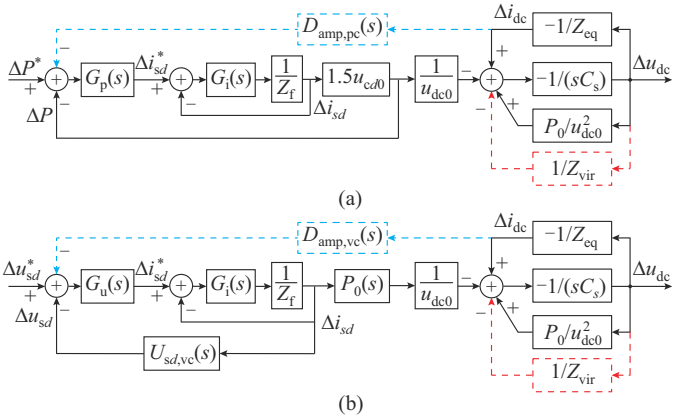

Fig. 4. Active damping of load converter station using DC-side current feedforward. (a) With power control. (b) With AC voltage control.

Take the load converter station with power control as an example. To achieve the virtual configuration of damping branch Z_{vir} in parallel with the DC-link capacitor, the active compensator can be obtained by the following two steps.

1) Equivalent Transformation

This step aims to acquire the compensator that is exactly equivalent to the damping branch Z_{vir}. Move the feedforward point from the part of the physical circuit to the outer control loop and the sampling point from Δu_{dc} to Δi_{dc}, the equivalent transformation of Z_{vir}, i.e., $D_{amp,pc}(s)$ marked by the blue dotted line, can be expressed as:

$$D_{amp,pc}(s)=\frac{u_{dc0}Z_{eq}}{Z_{vir}}\frac{1.5u_{cd0}G_p(s)G_i(s)+G_i(s)+Z_f}{1.5u_{cd0}G_p(s)G_i(s)}=\frac{u_{dc0}Z_{eq}}{Z_{vir}}\left(1+\frac{G_i(s)+Z_f}{1.5u_{cd0}G_p(s)G_i(s)}\right) \tag{20}$$

2) Simplified Implementation

This step aims to generate a practical compensator. As the inner current loop is generally configured with a large bandwidth, $G_i(s)/(G_i(s)+Z_f)$ can be regarded as a unity gain. To prevent the change of the steady-state operating point caused by the potential DC gain of the compensator, there are two methods to be selected: ① configuring an additional filter to remove the DC component, such as a high-pass and band-pass filter; and ② deleting the DC gain directly. To facilitate the implementation of the compensator, the second method is employed in this section, and the term $u_{dc0}Z_{eq}/Z_{vir}$ is removed. Thus, the compensator in (20) is finally reduced with a high-pass filter to the following form:

$$\hat{D}_{\text{amp,pc}}(s)=\frac{u_{\text{dc0}}Z_{\text{eq}}}{Z_{\text{vir}}}\frac{1}{1.5u_{cd0}G_{\text{p}}(s)}\approx\frac{k_{\text{f1}}s}{s+\omega_{\text{n1}}} \tag{21}$$

After the compensator in (21) is added to the load converter station with power control, according to Fig. 3(a), the reduced-order impedance model with active damping is expressed as:

$$Z_{\text{pc2,damp}}(s)=\frac{-(u_{\text{dc0}}+\hat{D}_{\text{amp,pc}}(s))G_{\text{p}}(s)H_1(s)+G_2(s)}{1-H_1(s)H_2(s)} \tag{22}$$

Similarly, the equivalent transformation of Z_{vir} used as the compensator with AC voltage control is exactly determined as:

$$D_{\text{amp,vc}}(s)=\frac{u_{\text{dc0}}Z_{\text{eq}}}{Z_{\text{vir}}}\frac{Z_{\text{f}}+G_{\text{i}}(s)+\dfrac{Z_{\text{load}}G_{\text{u}}(s)G_{\text{i}}(s)}{sC_{\text{f}}Z_{\text{load}}+1}}{P_0(s)G_{\text{u}}(s)G_{\text{i}}(s)} \tag{23}$$

If the filter capacitor is not considered, the active compensator can be simplified initially. By removing the inner current loop and DC gain, the compensator can be further obtained as:

$$\begin{aligned}\hat{D}_{\text{amp,vc}}(s)=&\frac{u_{\text{dc0}}Z_{\text{eq}}}{Z_{\text{vir}}}\frac{Z_{\text{f}}+G_{\text{i}}(s)+Z_{\text{load}}G_{\text{u}}(s)G_{\text{i}}(s)}{(1.5u_{cd0}+Z_{\text{load}}1.5i_{sd0})G_{\text{u}}(s)G_{\text{i}}(s)}=\\&\frac{u_{\text{dc0}}Z_{\text{eq}}}{Z_{\text{vir}}(1.5u_{cd0}+Z_{\text{load}}1.5i_{sd0})}\left(Z_{\text{load}}+\frac{Z_{\text{f}}+G_{\text{i}}(s)}{G_{\text{u}}(s)G_{\text{i}}(s)}\right)\approx\\&\frac{u_{\text{dc0}}Z_{\text{eq}}}{Z_{\text{vir}}(1.5u_{cd0}+Z_{\text{load}}1.5i_{sd0})}\left(Z_{\text{load}}+\frac{1}{G_{\text{u}}(s)}\right)\approx\frac{k_{\text{f2}}s}{s+\omega_{\text{n2}}}\end{aligned} \tag{24}$$

According to Fig. 3(b), the reduced-order impedance model with active damping applied to the load converter station under AC voltage control is given as:

$$Z_{\text{vc1,damp}}(s)=\frac{G_2(s)-\hat{D}_{\text{amp,vc}}(s)F_1(s)F_3(s)}{1-F_1(s)F_2(s)F_3(s)} \tag{25}$$

Remark 4: The above derivation process explains the origin of the compensator employed in this paper. Although the input impedance of the load converter station is remodeled after configuring the active damping, the reduced compensator is no longer exactly equivalent to the expected damping branch, and the suitability of the damping branch remains to be determined.

B. Parameter Design Based on Damping Factor Sensitivity

In the framework of impedance analysis, a parameter design method is proposed based on damping factor sensitivity and the equivalent cascade circuit shown in Fig. 1(b), where $Z_{\text{in}}(s)$ represents the input impedance of the load converter station with the active compensator configured. The current Δi_{dc} flowing from the background subsystem to the load converter station is expressed as:

$$\Delta i_{\text{dc}}=\left(V_{\text{s}}(s)+I_{\text{g}}(s)Z_{\text{in}}(s)\right)\Big/\left(Z_{\text{out}}(s)+Z_{\text{in}}(s)\right) \tag{26}$$

Given that the background subsystem is stable when unloaded, and the load converter station is stable when the background subsystem is short-circuit, i. e., $V_{\text{s}}(s)$ and $I_{\text{g}}(s)$ have no unstable poles, such that the stability of the current depends on $Z_{\text{out}}(s)$ and $Z_{\text{in}}(s)$. Note that the two assumptions made here are more relaxing than the classical assumptions of impedance analysis [15]. According to the pole distribution of $Z_{\text{out}}(s)$ and $Z_{\text{in}}(s)$, there are two cases that need to be treated differently.

1) Case 1: Both $Z_{\text{in}}(s)$ and $Z_{\text{out}}(s)$ Have No RHP Poles

In this case, both $Z_{\text{in}}(s)$ and $Z_{\text{total}}(s)=Z_{\text{out}}(s)+Z_{\text{in}}(s)$ have no RHP poles, and the stability of the current depends on the stability of the second term on the right-hand side of (26). If $Z_{\text{total}}(s)$ has no RHP zeros, then the system is stable. An approach commonly employed to assess the stability is to determine whether the Nyquist curve of $Z_{\text{total}}(s)$ surrounds the point (0, j0) [29].

Denote the intersection of the Nyquist curve of $Z_{\text{total}}(s)$ and the real axis as the resonance point. Thus, the real part at the resonance point is defined as the damping factor:

$$R_{\text{d}}=\text{Re}(Z_{\text{total}}(\text{j}\omega_{\text{n}})) \tag{27}$$

If $R_{\text{d}}<0$, the Nyquist curve of $Z_{\text{total}}(s)$ will surround the point (0, j0), thus indicating that the system is unstable. On the contrary, $R_{\text{d}}>0$ indicates that the system is stable. The value of R_{d} also represents the damping strength at the corresponding resonance point, which means that R_{d} has the function to guide the design of a satisfying compensator.

To achieve the sensitivity of R_{d}, $Z_{\text{total}}(s)$ should be arranged and its imaginary part can be further expressed as:

$$I_{\text{m}}=\frac{\sum_{i=0}^{n}A_i\omega^i}{\sum_{i=0}^{n}C_i\omega^i} \tag{28}$$

where n is the degree of the numerator plus that of the denominator in $Z_{\text{total}}(s)$; and A_i and C_i denote the coefficient terms after reorganization.

By solving $I_{\text{m}}=0$, we can obtain the resonant frequency ω_{m} and the damping factor at the resonant point can be given as:

$$R_{\text{d}}=\frac{\sum_{i=0}^{n}B_i\omega_{\text{m}}^i}{\sum_{i=0}^{n}C_i\omega_{\text{m}}^i} \tag{29}$$

where B_i is the corresponding coefficient terms.

The sensitivities of R_{d} to parameters k_{f} and ω_{n} used in the compensator can be expressed as:

$$\begin{cases}\dfrac{\partial R_{\text{d}}}{\partial k_{\text{f}}}=\dfrac{\sum_{i=0}^{n}\left(\dfrac{\partial B_i}{\partial k_{\text{f}}}\omega_{\text{m}}^i+iB_i\omega_{\text{m}}^{i-1}\dfrac{\partial\omega_{\text{m}}}{\partial k_{\text{f}}}\right)\sum_{i=0}^{n}C_i\omega_{\text{m}}^i-\sum_{i=0}^{n}B_i\omega_{\text{m}}^i\sum_{i=0}^{n}\left(\dfrac{\partial C_i}{\partial k_{\text{f}}}\omega_{\text{m}}^i+iC_i\omega_{\text{m}}^{i-1}\dfrac{\partial\omega_{\text{m}}}{\partial k_{\text{f}}}\right)}{\left(\sum_{i=0}^{n}C_i\omega_{\text{m}}^i\right)^2}\\[2ex]\dfrac{\partial R_{\text{d}}}{\partial\omega_{\text{n}}}=\dfrac{\sum_{i=0}^{n}\left(\dfrac{\partial B_i}{\partial\omega_{\text{n}}}\omega_{\text{m}}^i+iB_i\omega_{\text{m}}^{i-1}\dfrac{\partial\omega_{\text{m}}}{\partial\omega_{\text{n}}}\right)\sum_{i=0}^{n}C_i\omega_{\text{m}}^i-\sum_{i=0}^{n}B_i\omega_{\text{m}}^i\sum_{i=0}^{n}\left(\dfrac{\partial C_i}{\partial\omega_{\text{n}}}\omega_{\text{m}}^i+iC_i\omega_{\text{m}}^{i-1}\dfrac{\partial\omega_{\text{m}}}{\partial\omega_{\text{n}}}\right)}{\left(\sum_{i=0}^{n}C_i\omega_{\text{m}}^i\right)^2}\end{cases} \tag{30}$$

$$\begin{cases} \dfrac{\partial \omega_{\mathrm{m}}}{\partial k_{\mathrm{f}}} = -\dfrac{\sum_{i=0}^{n} \dfrac{\partial A_i}{\partial k_{\mathrm{f}}} \omega_{\mathrm{m}}^{i}}{\sum_{i=0}^{n} i A_i \omega_{\mathrm{m}}^{i-1}} \\ \dfrac{\partial \omega_{\mathrm{m}}}{\partial \omega_{\mathrm{n}}} = -\dfrac{\sum_{i=0}^{n} \dfrac{\partial A_i}{\partial \omega_{\mathrm{n}}} \omega_{\mathrm{m}}^{i}}{\sum_{i=0}^{n} i A_i \omega_{\mathrm{m}}^{i-1}} \end{cases} \tag{31}$$

Given that the compensator is configured by a group of initial parameters, if the system is still unstable, then the compensator parameters can be adjusted according to the direction indicated by the damping factor sensitivity. More specifically, the compensator parameter should be increased according to the setting step size when its damping factor sensitivity is greater than zero; otherwise, the compensator parameter should be decreased. After the multi-step adjustment until $R_{\mathrm{d}}>0$, it is necessary to verify the response of the MT-DC distribution system by configuring the compensator. If the response satisfies the requirements (such as response speed, overshoot) under the designed operating conditions, then the adjusting process ends and the appropriate compensator parameters are finally obtained. Such a process is similar to using the eigenvalue sensitivity of the state-space model to search for reasonable controller parameters.

2) Case 2: Either $Z_{\mathrm{in}}(s)$ or $Z_{\mathrm{out}}(s)$ Has RHP Poles

Either $Z_{\mathrm{in}}(s)$ or $Z_{\mathrm{out}}(s)$ has RHP poles, and the premise of using the damping factor R_{d} to determine the system stability does not exist, i.e., $V_{\mathrm{s}}(s)+I_{\mathrm{g}}(s)Z_{\mathrm{in}}(s)$ and $Z_{\mathrm{total}}(s)$ have no RHP poles, indicating that the method based on damping factor sensitivity is no longer valid. To ensure the applicability of the proposed method, supposing $Z_{\mathrm{in}}(s)$ or $Z_{\mathrm{out}}(s)$ has an RHP pole p_{x}, we can rearrange (26) into the following formulation.

$$\Delta i_{\mathrm{dc}} = \left[\left(V_{\mathrm{s}}(s)+I_{g}(s)Z_{\mathrm{in}}(s) \right) \frac{s-p_{\mathrm{x}}}{s+p_{\mathrm{x}}} \right] \frac{1}{\left(Z_{\mathrm{out}}(s)+Z_{\mathrm{in}}(s) \right) \dfrac{s-p_{\mathrm{x}}}{s+p_{\mathrm{x}}}} \tag{32}$$

Whether p_{x} is the RHP pole of $Z_{\mathrm{in}}(s)$ or $Z_{\mathrm{out}}(s)$, it is obvious that the first term on the right-hand side of (32) is stable. More specifically, if p_{x} is the RHP pole of $Z_{\mathrm{out}}(s)$, it does not affect the stability of the first term. If p_{x} is the RHP pole of $Z_{\mathrm{in}}(s)$, the pole is compensated by the corresponding zero of the same value. Thus, $\hat{Z}_{\mathrm{total}}(s)$ in (33) has the same stability characteristic as the original system.

$$\hat{Z}_{\mathrm{total}}(s) = \left(Z_{\mathrm{out}}(s)+Z_{\mathrm{in}}(s) \right) \frac{s-p_{\mathrm{x}}}{s+p_{\mathrm{x}}} \tag{33}$$

Based on the above zero-pole compensation, there are no RHP poles in $\hat{Z}_{\mathrm{total}}(s)$ such that the system stability and compensator parameter adjustment can be determined by the damping factor and its sensitivity. In a more general sense, if there are multiple RHP poles in $Z_{\mathrm{out}}(s)$ and $Z_{\mathrm{in}}(s)$, only multiple zero-pole compensations are required. By using the damping factor sensitivity, the flow chart of the adjusting process for the parameters of the active compensator is summarized as shown in Fig. 5.

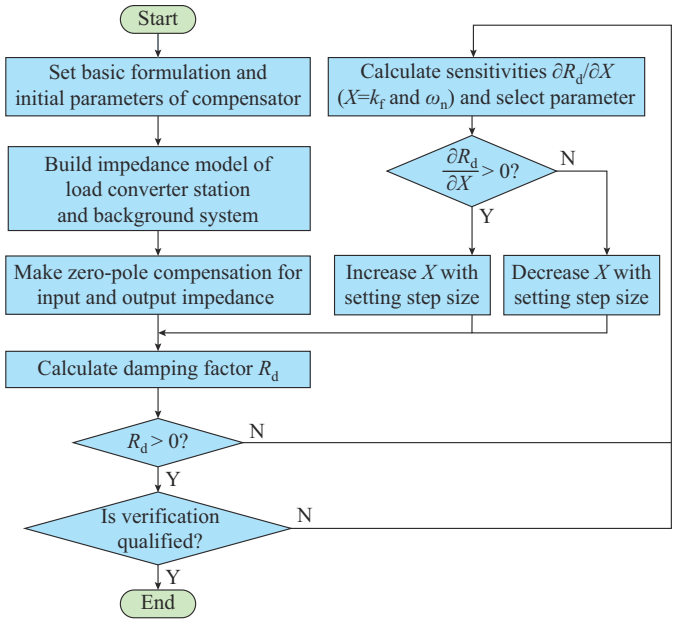

Fig. 5. Flow chart of adjusting process for parameters of active compensator.

Remark 5: in the stability assessment obtained by using the impedance analysis, the equivalent circuit of the load converter station can be flexibly selected on demand. For convenience of analysis, the load converter station in two control modes is represented by the Norton equivalent circuit. As shown in (22) and (25), since the compensator derived in Section III-A does not change the existing pole distribution of $Z_{\mathrm{in}}(s)$ after the configuration, all unstable poles in $Z_{\mathrm{in}}(s)$ and even $Z_{\mathrm{out}}(s)$ can be calculated in advance simultaneously.

IV. Case Studies

To verify the performance of the derived reduced-order impedance model and the parameter design method based on damping factor sensitivity, a three-terminal ±10 kV DC distribution system, as shown in Fig. 6, is employed in this section, of which the parameters are given in Table I, where k_{P} and k_{I} are the proportional and integral parameters, respectively. The rated capacities of stations 1 and 2 are 20 MVA and 10 MVA, respectively.

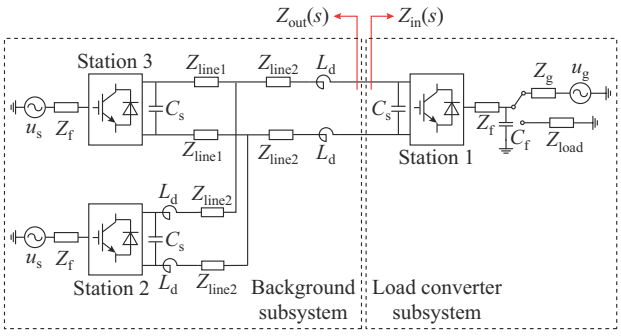

Fig. 6. Structure of three-terminal DC distribution system.

TABLE I
PARAMETERS OF MTDC DISTRIBUTION SYSTEM

Parameter	Value
Resistance of DC cable line in unit length	0.194 Ω/km
Inductance of DC cable line in unit length	0.625 mH/km
Resistance of inverter Z_f	1.3 mΩ
Inductance of inverter Z_f	3.22 mH
Current limiting reactor L_d	4 mH
Direct current capacitor C_s	1500 μF
Filter capacitor of AC side C_f	10 μH
k_p of outer power loop	0.1
k_i of outer power loop	10
k_p of outer voltage loop	0.2
k_i of outer voltage loop	10
k_p of inner current loop	5
k_i of inner current loop	80
Switching frequency	5000 Hz

A. Verification of Reduced-order Impedance Model

To verify the accuracy of the derived reduced-order model, the frequency sweep results of the DC-side impedance are taken as the reference. Figure 7(a) shows the comparison between sweep results S_{pc2} and the derived reduced-order impedance model with power control with and without damping, whereas Fig. 7(b) corresponds to the AC voltage control. The reduced-order impedance model agrees well with the frequency sweep results in the low- and middle-frequency bands. Owing to the neglect of the digital control delay, there is only a slight difference in the high-frequency band for the power control and AC voltage control with active damping. These results demonstrate the effectiveness of the derived DC-side reduced-order impedance models of the load converter station.

A further comparison of the reduced-order impedance models obtained by different methods is shown in Fig. 8. With respect to the power control, $Z_{pc1}(s)$ is accurate only at low frequencies compared with the full-order impedance $Z_{pc0}(s)$ because the physical quantities Δu_{cd} and Δi_{sq} are ignored, which implies that the derviation method of $Z_{pc1}(s)$ is inappropriate. As for the AC voltage control, there is little difference between the full-order impedance $Z_{vc0}(s)$, the reduced-order impedance $Z_{vc1}(s)$, and the negative resistance parallel with capacitor denoted by $Z_{vc2}(s)$, which is consistent with the theoretical analysis results. However, such a simplified impedance model represented by $Z_{vc2}(s)$ is invalid when considering the effect of the active compensator. It is worth noting that the input impedances corresponding to two control modes of load converter station both have an RHP pole, so the zero-pole compensation is required when the damping factor sensitivity is applied to the adjustment process of the compensator parameters.

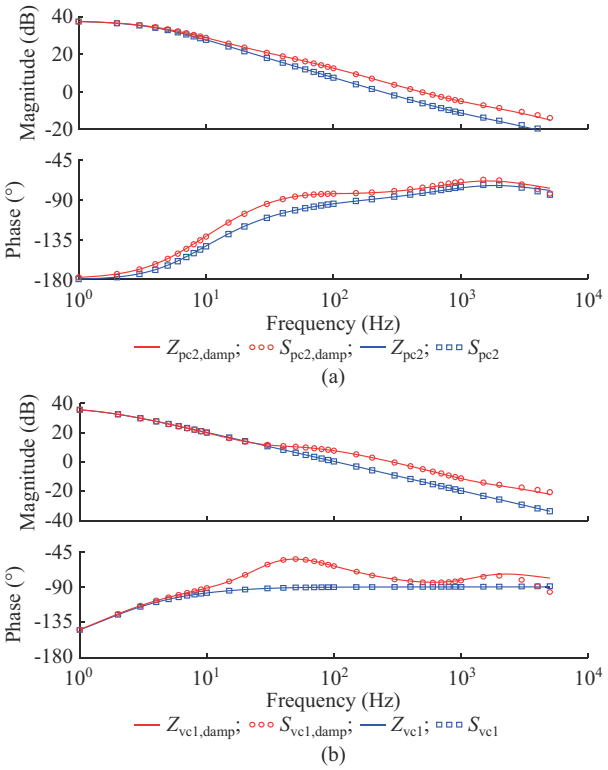

Fig. 7. Impedance comparison between sweep and derived reduced-order impedance model with and without damping. (a) With power control. (b) With AC voltage control.

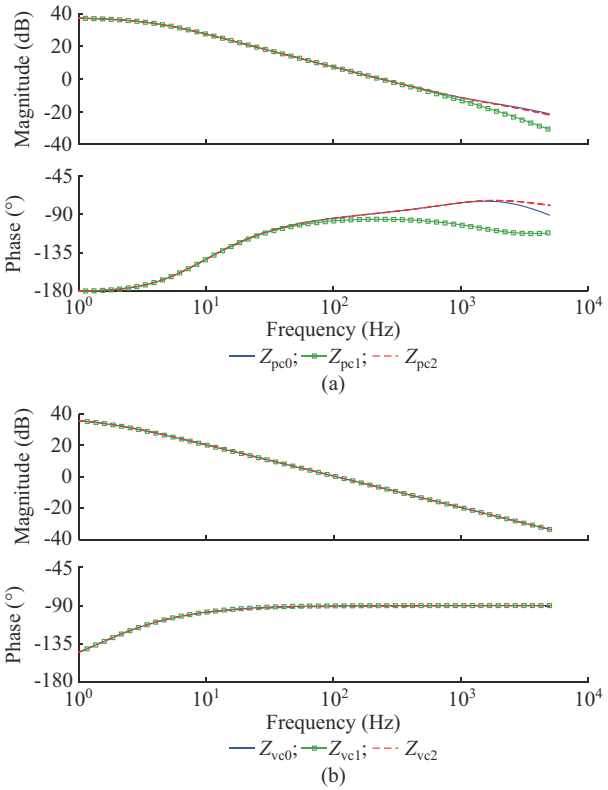

Fig. 8. Impedance comparison of load converter station using different derivation methods. (a) With power control. (b) With AC voltage control.

B. Verification for Parameter Design of Active Damping

For the load converter station with power control, Fig. 9(a) shows the variation in the values of the damping factor sensitivity with the compensator parameter ω_n, and Fig. 9(b) depicts the values of the damping factor, whereas Fig. 10 corresponds to the compensator parameter k_f. When the active compensator is not employed ($k_f=0$), R_d is less than 0 and the system is unstable. When the compensator is enabled (k_f is a nonzero constant), R_d increases at first and then decreases as ω_n increases. The sensitivity values of R_d indicate the increase and decrease speeds, which are highly consistent with the variation of R_d. Let ω_n be a constant, the sensitivity of R_d to k_f also exhibits a similar performance, which indicates that the proposed damping factor sensitivity can be used in the design of compensator parameters.

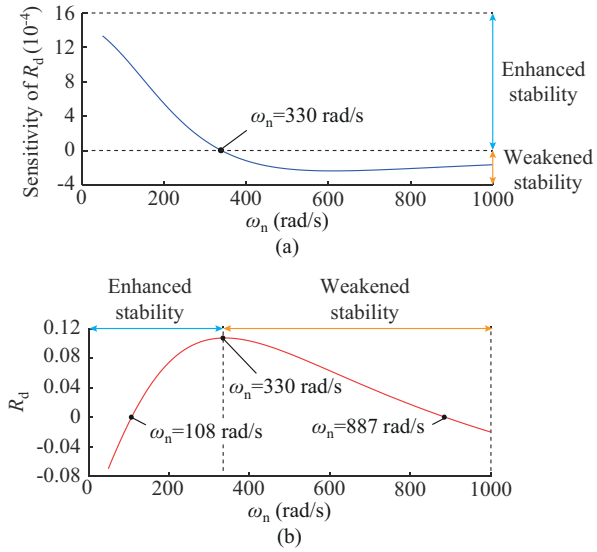

Fig. 9. Sensitivity of damping factor R_d to ω_n and values of R_d under power control. (a) Sensitivity of R_d to ω_n. (b) Variation of R_d with ω_n.

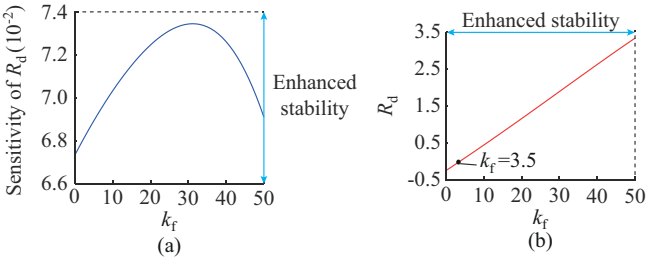

Fig. 10. Sensitivity of damping factor R_d to k_f and values of R_d under power control. (a) Sensitivity of R_d to k_f. (b) Variation of R_d with k_f.

To further illustrate the significance of the damping factor sensitivity, the sensitivity of the dominant eigenvalue in the state-space model is used as a comparison. Figure 11(a) and (b) shows the sensitivity of the real part of dominant eigenvalue to the compensator parameter ω_n and the trajectory of the real part of dominant eigenvalue with the change of ω_n, respectively, whereas Fig. 12 corresponds to the compensator parameter k_f. It is well-known that the real part of the dominant eigenvalue reflects the asymptotic stability of the system. When the real part of the dominant eigenvalue is less than 0, the system is stable, which is the opposite of judging stability by $R_d>0$.

As shown in Figs. 11 and 12, the change trends of the sensitivity and dominant eigenvalue (real part) are opposite to those shown in Figs. 9 and 10, respectively, and the stability limits are completely consistent. Therefore, the damping factor sensitivity and the eigenvalue sensitivity are equivalent to some extent. However, the latter solution relies on a complete state-space small-signal model, while the former employs the reduced-order impedance model, which is easy to adopt.

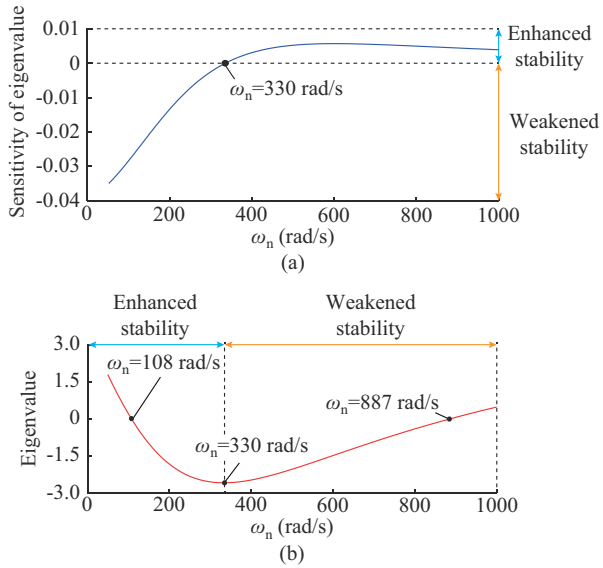

Fig. 11. Sensitivity of dominant eigenvalue to ω_n and trajectory of dominant eigenvalue under power control (k_f=5). (a) Sensitivity of dominant eigenvalue to ω_n. (b) Trajectory of real part of dominant eigenvalue.

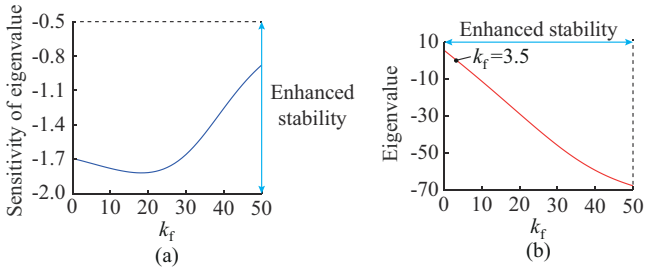

Fig. 12. Sensitivity of dominant eigenvalue to k_f and trajectory of dominant eigenvalue under power control. (a) Sensitivity of dominant eigenvalue to k_f. (b) Trajectory of real part of dominant eigenvalue.

By combining different parameters, Table II summarizes different compensators and their small-signal stability, where the red part indicates that the system is stable.

TABLE II
DIFFERENT COMBINATIONS OF COMPENSATOR PARAMETERS AND THEIR SMALL-SIGNAL STABILITY

ω_n (rad/s)	Transfer function of compensator		
	$k_f=3$	$k_f=4$	$k_f=5$
100	$3s/(s+100)$	$4s/(s+100)$	$5s/(s+100)$
200	$3s/(s+200)$	$4s/(s+200)$	$5s/(s+200)$
330	$3s/(s+330)$	$4s/(s+330)$	$5s/(s+330)$

Figures 13 and 14 depict the time-domain simulation results under the power disturbance of station 1 with different combinations of compensator parameters. When $t=1.0$ s, the power step reaches 20 MW, and the DC voltage and current start to diverge and oscillate, such that the system loses stability. After the designed active compensator is enabled, the time-domain simulation results are consistent with the analysis result using the damping factor. When the designed compensator is enabled, R_d is greater than zero, and thus the oscillation converges gradually; otherwise, it continues to diverge.

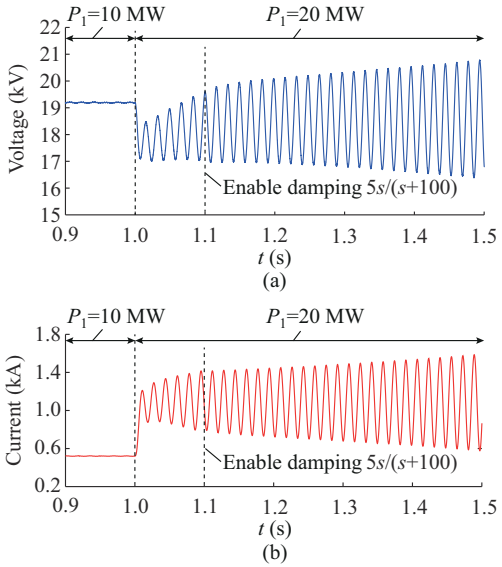

Fig. 13. Simulation results of step response when station 1 employs power control with active compensator $5s/(s+100)$. (a) DC-side voltage. (b) Input current.

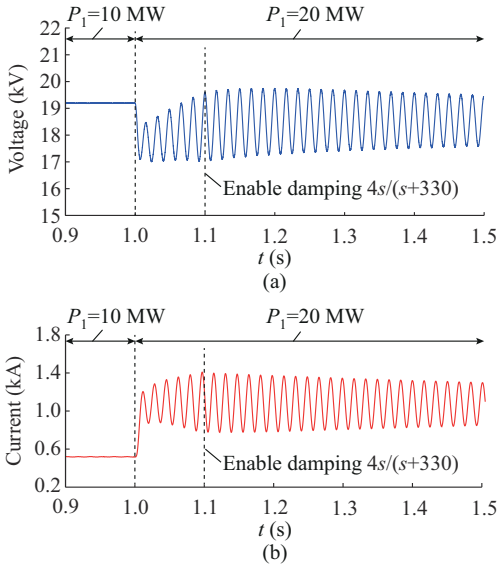

Fig. 14. Simulation results of step response when station 1 employs power control with active compensator $4s/(s+330)$. (a) DC-side voltage. (b) Input current.

Considering the actual requirements of damping and response speed, the appropriate compensator parameters are obtained after the multi-step adjustment and verification, namely, $33s/(s+330)$. Figure 15 illustrates the Nyquist curve of $Z_{total}(s)$, and its stability assessment result is consistent with that obtained by using R_d. Figure 16 depicts the time-domain simulation result under the power disturbance of station 1. Both the stability and response speed can meet the requirements.

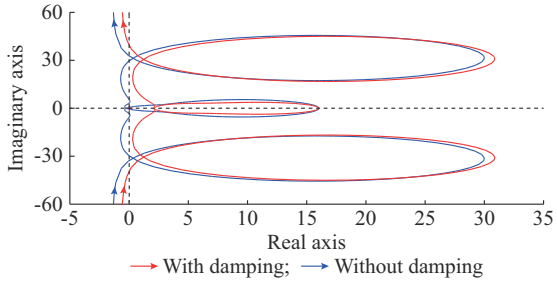

Fig. 15. Nyquist plots of Z_{total} under power control with active compensator $33s/(s+330)$.

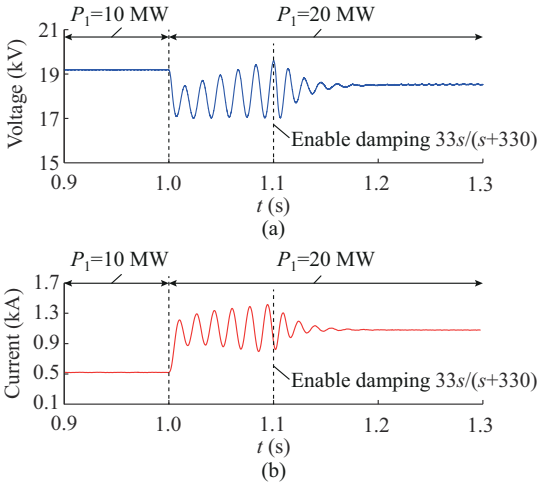

Fig. 16. Simulation results of step response when station 1 adopts power control with active compensator $33s/(s+330)$. (a) DC-side voltage. (b) Input current.

Figures 17-20 show the analysis and simulation results of load converter station with AC voltage control, and the phenomenon is consistent with the power control, which is not explained in detail because of limited space.

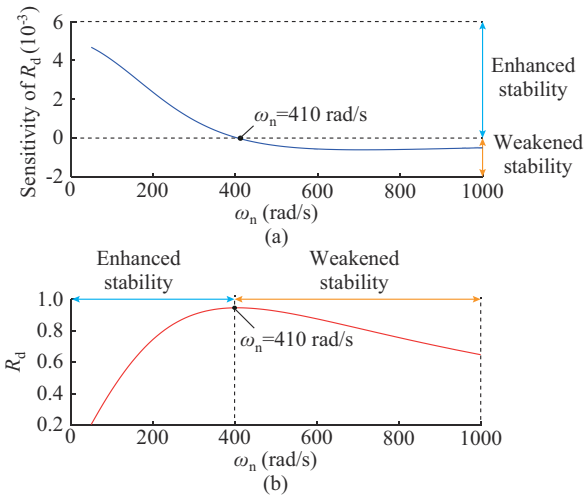

Fig. 17. Sensitivity of damping factor R_d to ω_n and value of R_d under AC voltage control ($k_f=5$). (a) Sensitivity of R_d to ω_n. (b) Value of R_d with ω_n.

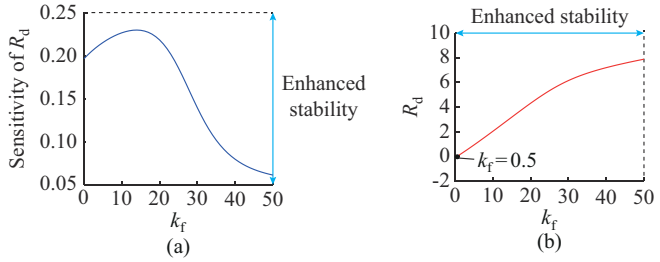

Fig. 18. Sensitivity of damping factor R_d to k_f and value of R_d under AC voltage control. (a) Sensitivity of R_d to k_f. (b) Variation of R_d with k_f.

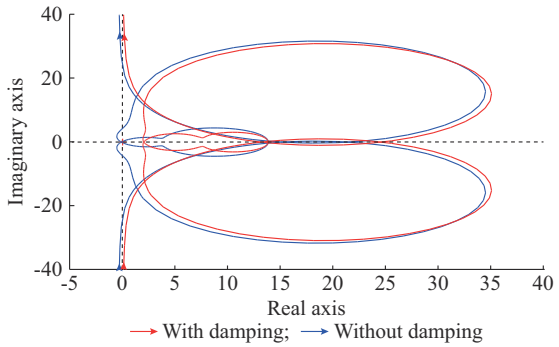

Fig. 19. Nyquist plots of Z_{total} under AC voltage control with and without active compensator $10s/(s+410)$.

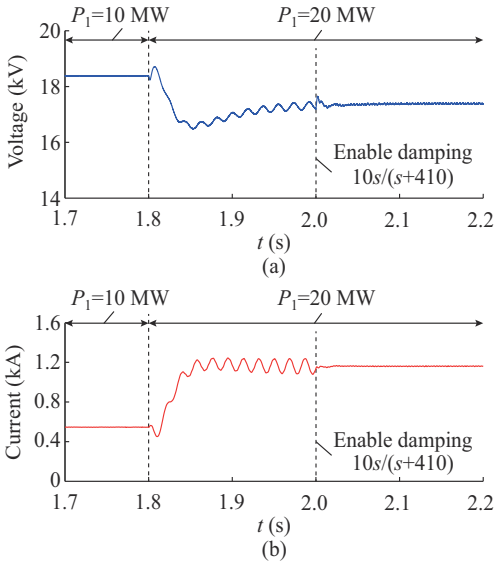

Fig. 20. Simulation results of step response when station 1 adopts AC voltage control with active compensator. (a) DC-side voltage. (b) Input current.

With the power control employed in both stations 1 and 2, the comparison with and without active damping is shown in Fig. 21. Figure 22 shows the comparison with and without active compensator when station 1 employs AC voltage control and station 2 employs power control. When the active compensator is not enabled, the DC voltage and current have resonant oscillations because of the power fluctuations. Once the active compensator is put into operation, the resonance oscillation on the DC side is effectively suppressed, and the DC voltage and current waveforms become smooth, which illustrates the effectiveness of the designed active compensator.

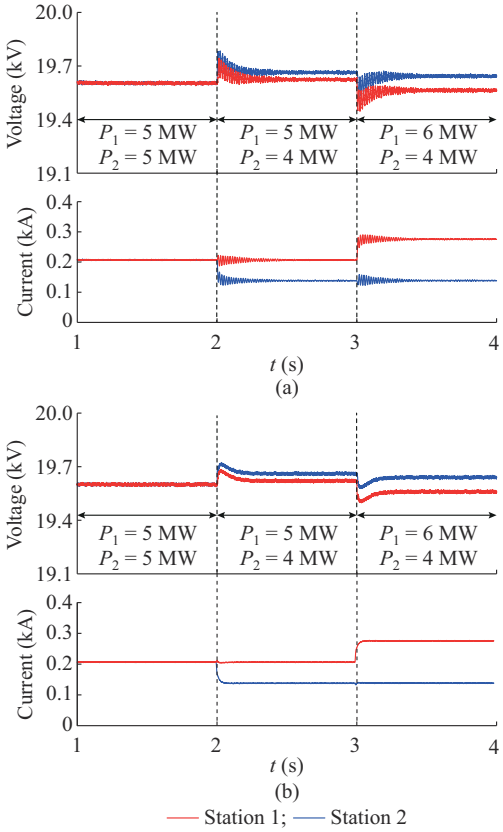

Fig. 21. Voltage and current dynamics of system when stations 1 and 2 adopts power control. (a) Without active damping. (b) With active damping.

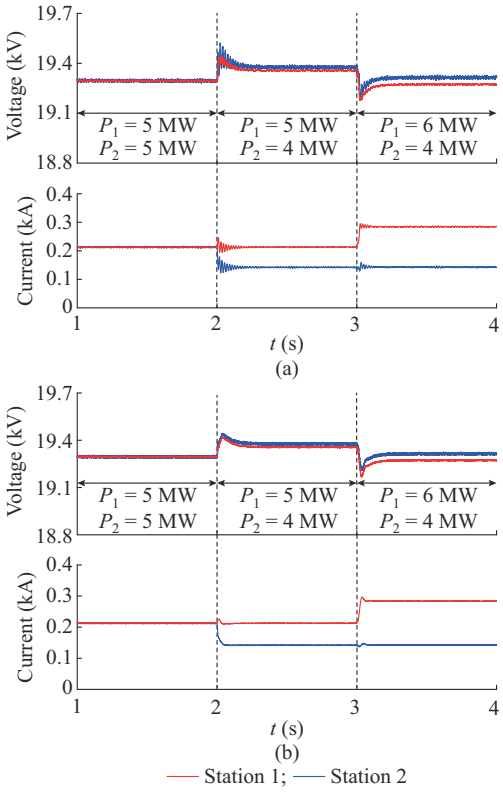

Fig. 22. Voltage and current dynamics of system when station 1 adopts AC voltage control and station 2 employs power control. (a) Without active damping. (b) With active damping.

C. Hardware-in-the-Loop (HIL) Experiments

The control HIL experiment, as an efficient test tool widely used in complex converter-dominated power system, is adopts to reflect the actual performance of the digital controller with a designed active compensator, which is carried out based on the digital signal processing (DSP) control board and circuit simulator, as shown in the Appendix A. The parameters used in the circuit simulator and the digital controller are shown in Table III. It should be noted that owing to the limitation with respect to circuit simulators, the simulation step is set up to 20 μs and the sampling interval is 30 μs. Compared with the off-line simulation using MATLAB/Simulink, the simulation step and sampling interval of the HIL experiment are significantly increased. Even though the main circuit parameters remain unchanged, the PI parameters are still required to decrease owing to the increase in the integration time step.

After the multi-step parameter adjustment using the proposed method based on impedance and damping factor sensitivity, the compensator parameters of a load converter station with power control and AC voltage control are designed as $34s/(s+340)$ and $10s/(s+410)$, respectively. Figures 23-26 show the experimental results for station 1 with two control modes, which are obtained by setting the power step from 10 MW to 20 MW at the load converter station. The performances are consistent with the off-line simulation results, where the divergence oscillation of the DC voltage and current converges rapidly after the compensator is enabled. If the active compensator is configured from the beginning, the voltage and current do not oscillate and diverge.

TABLE III
PARAMETERS OF HIL EXPERIMENT

Parameter	Value
k_P of outer loop (power control)	0.1
k_I of outer loop (power control)	10
k_P of outer loop (AC voltage control)	0.2
k_I of outer loop (AC voltage control)	10
k_P of inner loop (power control)	3
k_I of inner loop (power control)	10
k_P of inner loop (AC voltage control)	4.6
k_I of inner loop (AC voltage control)	10
Simulation step	20 μs
Sampling interval	30 μs
Switching frequency	2500 Hz

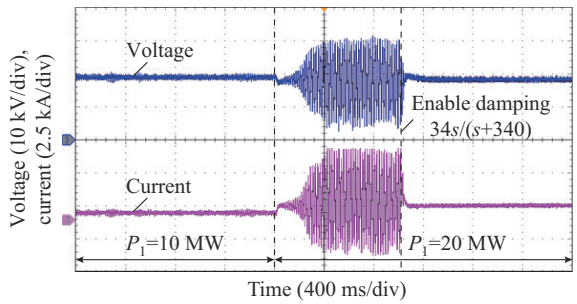

Fig. 23. Experimental results of step response when station 1 adopts power control (enable damping).

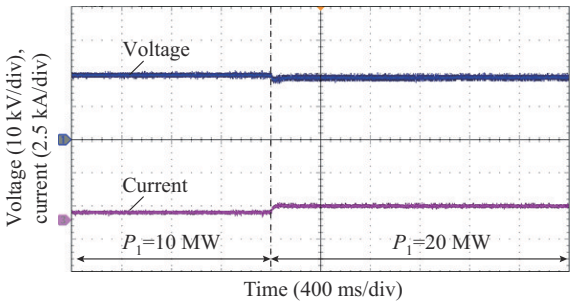

Fig. 24. Experimental results of step response when station 1 adopts power control (with damping from the beginning).

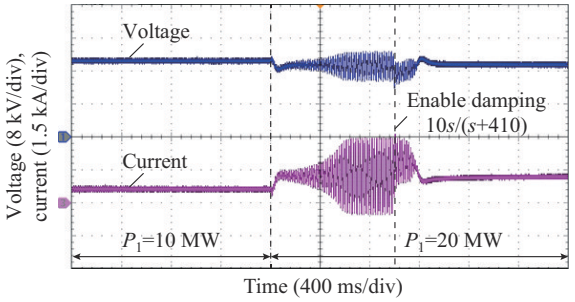

Fig. 25. Experimental results of step response when station 1 adopts AC voltage control (enable damping).

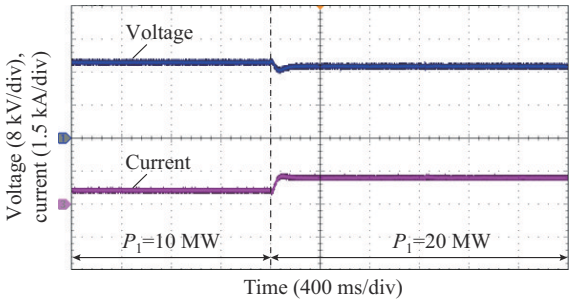

Fig. 26. Experimental results of step response when station 1 adopts AC voltage control (with damping from the beginning).

V. CONCLUSION

Starting from the DC-side small-signal impedance modeling of a load converter station, this paper investigates the application of reduced-order impedance models and an effective active compensator to power control and AC voltage control. In the framework of impedance analysis, a method based on reduced-order impedance and damping factor sensitivity to design the compensator parameter is further proposed. The accuracy of the derived reduced-order model and the effectiveness of the proposed method are verified by the three-terminal DC distribution system using a time-domain simulation and frequency-domain analysis. Some conclusions are derived as follows.

1) The reduced-order model of the load converter station should take into account the input quantity of the power stage as much as possible.

2) The characteristic of damping factor sensitivity is similar to that of eigenvalue sensitivity, which possesses the function of indicating the direction of stability enhancement

with a change in the compensator parameters.

3) The parameter design method based on damping factor sensitivity is compatible with the framework of impedance analysis, such that it can be easily implemented in nature.

APPENDIX A

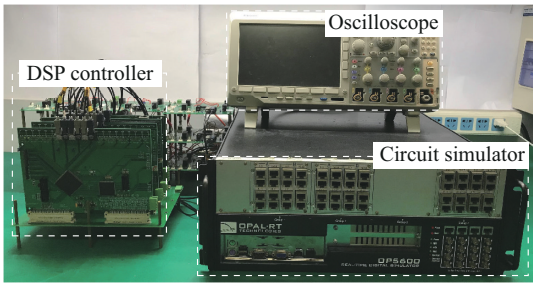

Fig. A1. Experimental platform.

REFERENCES

[1] S. Golestan, E. Ebrahimzadeh, B. Wen *et al*., "*dq*-frame impedance modeling of three-phase grid-tied voltage source converters equipped with advanced PLLs," *IEEE Transactions on Power Electronics*, vol. 35, no. 3, pp. 3524-3539, Mar. 2021.

[2] T. Hakala, T. Lahdeaho, and P. Jarventausta, "Low-voltage DC distribution-utilization potential in a large distribution network company," *IEEE Transactions on Power Delivery*, vol. 30, no. 4, pp. 1694-1701, Aug. 2015.

[3] J. Liu, X. Huang, Y. Hong *et al*., "Coordinated control strategy for operation mode switching of DC distribution networks," *Journal of Modern Power Systems and Clean Energy*, vol. 8, no. 2, pp. 334-344, Mar. 2020.

[4] H. Liu, Y. Wang, M. Wang *et al*., "Small-signal analysis of DC microgrid and multi-objective optimization segmented droop control suitable for economic dispatch," *Journal of Modern Power Systems and Clean Energy*, vol. 8, no. 3, pp. 564-572, May 2020.

[5] A. Emadi, A. Khaligh, C. Rivetta *et al*., "Constant power loads and negative impedance instability in automotive systems: definition, modeling, stability, and control of power electronic converters and motor drives," *IEEE Transactions on Vehicular Technology*, vol. 55, no. 4, pp. 1112-1125, Jul. 2006.

[6] M. Wu and D. Lu, "A novel stabilization method of LC input filter with constant power loads without load performance compromise in DC microgrids," *IEEE Transactions on Industrial Electronics*, vol. 62, no. 7, pp. 4542-4562, Jul. 2015.

[7] J. Beerten, S. D'Arco, and J. A. Suul, "Identification and small-Signal analysis of interaction modes in VSC MTDC systems," *IEEE Transactions on Power Delivery*, vol. 31, no. 2, pp. 888-897, Apr. 2016.

[8] W. Zhao, P. Chen, X. Chen *et al*., "AC current feedback damping control strategy for VSC converter station in multi-terminal DC distribution system," *Proceedings of the CSEE*, vol 41, no. 10, pp. 3505-3517, May 2021.

[9] X. Lan, K. Sun, J. M. Guerrero *et al*., "Stability enhancement based on virtual impedance for DC microgrids with constant power loads," *IEEE Transactions on Smart Grid*, vol. 6, no. 6, pp. 2770-2783, Nov. 2015.

[10] B. Qin, W. Liu, R. Zhang *et al*., "Small-signal stability analysis and optimal control parameters design of MMC-based MTDC transmission systems," *IET Generation, Transmission & Distribution*, vol. 14 no. 21, pp. 4675-4683, Jan. 2020.

[11] G. O. Kalcon, G. P. Adam, O. Anaya-Lara *et al*., "Small-signal stability analysis of multi-terminal VSC-based DC transmission systems," *IEEE Transactions on Power Systems*, vol. 27, no. 4, pp. 1818-1830, Nov. 2012.

[12] S. Shah and L. Parsa, "Impedance modeling of three-phase voltage source converters in *dq* sequence, and phasor domains," *IEEE Transactions on Energy Conversion*, vol. 32, no. 3, pp. 1139-1150, Sept. 2017.

[13] C. E. Ugalde-Loo, J. B. Ekanayake, and N. Jenkins, "State-space modeling of wind turbine generators for power system studies," *IEEE Transactions on Industry Applications*, vol. 49, no. 1, pp. 223-232, Jan.-Feb. 2013.

[14] N. Kroutikova, C. A. Hernandez-Aramburo, and T. C. Green, "State-space model of grid-connected inverters under current control mode," *IET Electric Power Applications*, vol. 1, no. 3, pp. 329-338, May 2007.

[15] J. Sun, "Impedance-based stability criterion for grid-connected inverters," *IEEE Transactions on Power Electronics*, vol. 26, no. 11, pp. 3075-3078, Nov. 2011.

[16] M. Cespedes and J. Sun, "Impedance modeling and analysis of grid-connected voltage-source converters," *IEEE Transactions on Power Electronics*, vol. 29, no. 3, pp. 1254-1261, Nov. 2014.

[17] L. Xu, L. Fan, and Z. Miao, "DC impedance-model-based resonance analysis of a VSC-HVDC system," *IEEE Transactions on Power Delivery*, vol. 30, no. 3, pp. 1221-1230, Jun. 2015.

[18] G. Pinares and M. Bongiorno, "Modeling and analysis of VSC-based HVDC systems for DC network stability studies," *IEEE Transactions on Power Delivery*, vol. 31, no. 2, pp. 848-856, Apr. 2016.

[19] D. Xue, J. Liu, Z. Liu *et al*., "Modeling and analysis of DC terminal impedance of voltage-source converters with different control modes," *IEEE Transactions on Power Electronics*, vol. 35, no. 6, pp. 5883-5896, Jun. 2020.

[20] Z. Li, Z. Wang, Y. Wang *et al*., "Accurate impedance modeling and control strategy for improving the stability of DC system in multi-terminal MMC-based DC grid," *IEEE Transactions on Power Electronics*, vol. 35, no. 10, pp. 10026-10049, Oct. 2020.

[21] W. Wu, Y. Chen, A. Luo *et al*., "A virtual phase-lead impedance stability control strategy for the maritime VSC-HVDC system," *IEEE Transactions on Informatics*, vol. 14, no. 12, pp. 5475-5486, Dec. 2018.

[22] Y. Jin and X. Dong, "Small-signal stability analysis of dc distribution network adopting droop control," *Automation of Electric Power Systems*, vol. 40, no. 14, pp. 78-85, Jul. 2016.

[23] X. Li, L. Guo, D. Huang *et al*., "A reduced RLC impedance model for dynamic stability analysis of pi controller based DC voltage control of generic source-load two-terminal DC systems," *IEEE Journal of Emerging and Selected Topics in Power Electronics*, doi: 10.1109/JESTPE.2020.3016059

[24] L. Zhou, W. Wu, Y. Chen *et al*., "Virtual positive-damping reshaped impedance stability control method for the offshore MVDC system," *IEEE Transactions on Power Electronics*, vol. 34, no. 5, pp. 4951-4966, May 2019.

[25] D. Yang, X. Ruan, and H. Wu, "Impedance shaping of the grid-connected inverter with LCL filter to improve its adaptability to the weak grid condition," *IEEE Transactions on Power Electronics*, vol. 29, no. 11, pp. 5795-5805, Oct. 2014.

[26] X. Chen, Y. Zhang, and Y. Wang, "A study of dynamic interaction between PV grid-connected inverters and grid based on the impedance analysis method," *Proceedings of the CSEE*, vol. 34, no. 27, pp. 4559-4567, Sept. 2014.

[27] J. Zhou, H. Ding, S. Fan *et al*., "Impact of short-circuit ratio and phase-locked-loop parameters on the small-signal behavior of a VSC-HVDC converter," *IEEE Transactions on Power Delivery*, vol. 29, no. 5, pp. 2287-2296, Oct. 2014.

[28] A. Yazdani and R. Iravani, *Voltage-sourced Converters in Power Systems: Modeling, Control and Applications*. Hoboken: IEEE Press, 2010.

[29] M. Amin, M. Molinas, L. Jing *et al*., "Impact of power flow direction on the stability of VSC-HVDC seen from the impedance Nyquist plot," *IEEE Transactions on Power Electronics*, vol. 32, no. 10, pp. 8204-8217, Oct. 2017.

Pengwei Chen received the B.S. and Ph.D degrees in electrical engineering from North China Electric Power University, Beijing, China, in 2014 and 2019, respectively. From 2017 to 2018, he was a Visiting Scholar at the Future Renewable Electric Energy Delivery and Management (FREEDM) Systems Center, North Carolina State University, Raleigh, USA. He is presently a Lecturer at Nanjing University of Aeronautics and Astronautics, Nanjing, China. His research interests include DC distribution network simulation, stability, and power quality control.

Wenmeng Zhao received the B.S. degree in electrical engineering from Dalian University of Technology, Dalian, China, in 2019. She is currently working towards the Ph.D degree in electrical engineering at Nanjing University of Aeronautics and Astronautics, Nanjing, China. Her research interests include DC distribution network modeling, control, and stability analysis.

Xin Chen received the B.S. and Ph.D degrees in electrical engineering from Nanjing University of Aeronautics and Astronautics, Nanjing, China, in 1996 and 2001, respectively. From 2010 to 2011, he was a Visiting Scholar with the Rensselaer Polytechnic Institute, Troy, USA. He is currently a Professor at the Nanjing University of Aeronautics and Astronautics. His research interests include power electronics and energy conversion, with a focus on modeling, control, stability as well as applications in renewable energy systems.

Wenwei Jiang received the B.S. degree in electrical engineering from Jiangsu University of Science and Technology, Zhenjiang, China, in 2020. He is currently working towards the M.S. degree in electrical engineering at Nanjing University of Aeronautics and Astronautics, Nanjing, China. His research interests include renewable energy generation technology and DC distribution network modeling.